

High resolution measurement of tagged two-neutron energy and angle correlations in ^{252}Cf (sf)

P. F. Schuster^{a,*}, M. J. Marcath^a, S. Marin^a, S. D. Clarke^a, M. Devlin^b, R. C. Haight^b,
R. Vogt^{c,d}, P. Talou^b, I. Stetcu^b, T. Kawano^b, J. Randrup^e, S. A. Pozzi^a

^a*Department of Nuclear Engineering and Radiological Sciences, University of Michigan, Ann Arbor, MI 48109, USA*

^b*T-2, Los Alamos National Laboratory, Los Alamos, New Mexico, 87545, USA*

^c*Nuclear and Chemical Sciences Division, Lawrence Livermore National Laboratory, Livermore, CA 94551, USA*

^d*Department of Physics, University of California, Davis, California 95616, USA*

^e*Nuclear Science Division, Lawrence Berkeley National Laboratory, Berkeley, CA, USA*

Abstract

Background: Spontaneous fission events emit prompt neutrons correlated with one another in emission angle and energy. Measurements of these correlations can shed light on the partitioning of the excitation energy between the fragments, even if they are not directly measured.

Purpose: We explore the relationship in energy and angle between correlated prompt neutrons emitted from ^{252}Cf spontaneous fission.

Methods: Measurements with the Chi-Nu array provide experimental data for coincident neutrons tagged with a fission chamber signal with 10° angular resolution and 1 ns timing resolution for time-of-flight energy calculations. The experimental results are compared to simulations produced by the fission event generators CGMF, FREYA, and MCNPX-POLIMI IPOL(1)=1.

Results: We find that the measurements and the simulations all exhibit anisotropic neutron emission, although differences between fission event generators are evident.

Conclusions: This work shows that the dependence of detected neutron energy on the energy of another neutron detected in coincidence, although weak, is non-negligible, indicating that there may be correlations in energy between two neutrons emitted in the same fission event.

Keywords: Fission, Neutron, Correlation

1. Introduction

In a fission event, prompt neutron emission occurs on a time scale shorter than that of gamma-ray emission [1, 2]. The emitted neutrons are correlated with one another in their emission angle

*Corresponding author.
Preprint submitted to Physical Review C
Email address: pfschus@umich.edu (P. F. Schuster)

and energy [3, 4]. Measurements of these correlations can shed light on the partitioning of the excitation energy between the fragments, even if they are not directly measured. The commonly used MCNPX-PoliMi Monte Carlo code treats such correlations using data-based evaluations [5]. The new, physics-based fission models CGMF [6, 7, 8] and FREYA [9, 10, 11, 12, 13, 14, 15] generate complete events and can thus produce correlations between emitted particles on an event-by-event basis. These codes require high fidelity experimental data for validating their models. In this paper, we describe our ^{252}Cf spontaneous fission data, correlated in neutron energy and two-neutron angular separation, and compare the measured correlations to those simulated with the fission models MCNPX-PoliMi, CGMF, and FREYA, each using MCNPX-PoliMi for radiation transport and MPPost [16] for detector response.

Numerous detector systems exist or are in development for nuclear nonproliferation, safeguards, and arms control applications that would benefit from a better understanding of the correlations in prompt fission neutron emission. One such example is the fast neutron multiplicity counter, a nuclear safeguards instrument that is used for nondestructive assay of special nuclear material [18, 19]. Similarly, applications have been proposed for exploiting the correlations that exist between neutrons emitted from the same fission event in multiplying materials where fission chains are present [20, 21]. Accurate physics models are important in the development of these systems and methods.

This paper presents measurements and simulations of correlated neutrons from ^{252}Cf spontaneous fission to confirm and extend previously reported results. Measurements were made with 42 detectors of the Chi-Nu detector array at the Los Alamos Neutron Science Center (LANSCE) at Los Alamos National Laboratory (LANL) [22, 23]. The Chi-Nu array covers a large solid angle with detectors approximately 1 m from the source, thereby providing high efficiency and excellent timing resolution for time-of-flight energy calculations. Additionally, the ^{252}Cf source was embedded in a fission chamber, providing good time resolution for the fission event signal. Double coincident neutron events, in which two neutrons are detected in coincidence with a fission chamber trigger, were identified as “bicorrelation” events, as explained in Sec. 2.3. The measurement offers improved angle resolution, excellent timing resolution, and enhanced background suppres-

sion compared to previous work [4, 24]. A previous paper by the authors investigated correlations between the prompt neutron and photon multiplicities [25]. This work includes the first comparison of correlated neutron energy characteristics for ^{252}Cf spontaneous fission, including a new observable: the average energy of neutrons detected in coincidence with emitted neutrons at a given energy as a function of the angle between them.

2. Experimental, Simulation, and Analysis Methods

2.1. Measurement Setup and Methods

In this work, we employ the data taken with the Chi-Nu detector array, illustrated in Fig. 1, at the LANL LANSCE facility in 2015, using a ^{252}Cf spontaneous fission source, for our bicornelation analysis. Because the experimental setup for this analysis was described in detail in Refs. [25, 23], we only briefly summarize the parts of the setup relevant for this analysis here. The Chi-Nu array consists of 54 EJ309 liquid scintillator detectors mounted at 15° intervals along six arcs to form a hemispherical distribution of detectors. Each detector is cylindrical, 17.78 cm in diameter and 5.08 cm thick, coupled to a 12.7 cm diameter photomultiplier tube (Hamamatsu R4144). Each detector subtends approximately a 10° angle from the source. Limitations in the acquisition system constrained these measurements to using only 42 detectors, making for 861 pairs of detectors at angles from 15° to 180° . The large number of detector pairs produces a wide range of angles, allowing for discretization in 10° bins, as shown in Fig. 2, which is improved compared to previous work with only 30° or 90° resolution [4, 20]. Each 10° bin contains multiple detector pairs. The standard deviation of detector pair angles within each bin is represented as the bar color in Fig. 2. Observable quantities are averaged across all pairs within a bin to reduce statistical error per bin.

A ^{252}Cf (sf) source was embedded in a fission chamber, with characteristics detailed in Ref. [25]. To summarize, the Californium source was deposited over a hemispherical chamber. One or two fragments from a fission event may produce a pulse by escaping the surface and depositing energy through ionization. This trigger signal was used as the fission time t_0 for each detected event, as explained in Sec. 2.3. The fission chamber has a fixed threshold to exclude α -particle interactions [30]. The source was fabricated in 2010 and the measurements reported here were

85 performed in 2015. The ^{252}Cf spontaneous fission count rate was 2.98×10^5 spontaneous fissions
 86 per second, with negligible contributions from spontaneous fission of ^{250}Cf and ^{248}Cm . The source
 87 was placed at the focal point of the hemispherical array so that the detectors were approximately
 88 1 m from the source. Over the duration of the measurement, 2.2×10^9 fission events occurred,
 89 resulting in 1.42×10^9 fission chamber triggers.

90 The use of the fission chamber makes this measurement unique compared to similar measure-
 91 ments made in the past because it provides a reference time for when a fission event occurs.
 92 Thus the neutron time-of-flight may be directly calculated for each detected neutron whereas
 93 previous work was limited to calculating the difference between the detection times of correlated
 94 particles [4].

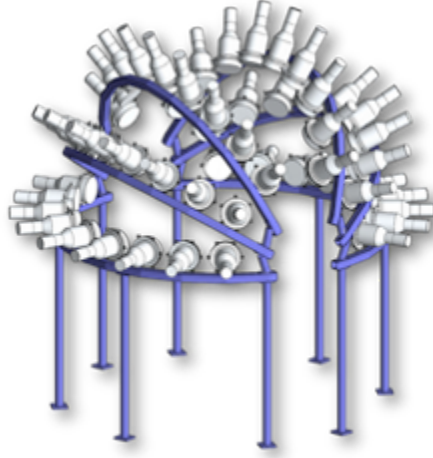


Figure 1: Diagram of the Chi-Nu detector array of 54 detectors. For this work, only 42 detectors were used.

95 Full waveforms were recorded with three CAEN V1730 digitizers with 500 MHz sampling and
 96 14-bit amplitude resolution over a 2 V range and post-processed in digital form. Standard digital
 97 pulse processing was implemented, as detailed in Ref. [25]. Particle types were classified using
 98 charge-integration n - γ pulse shape discrimination (PSD) [26], which was performed offline and
 99 optimized uniquely for each detector. A quadratic PSD line was used to discriminate between the
 100 neutrons and photons with misclassification of low light output events estimated to be approxi-
 101 mately 1% of all measured events.

102 The measurement had a pulse height threshold of 100 keVee (“electron-equivalent” keV) light
 103 output, corresponding to approximately 0.8 MeV neutron energy deposited. This threshold was

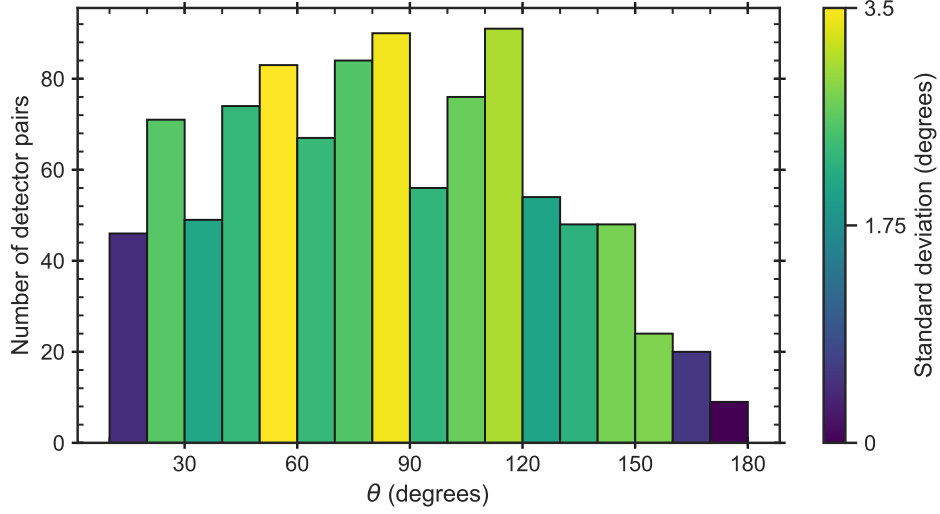


Figure 2: Visualization of detector pair angle distribution, discretized to 10° bins. The height of each bar shows the number of detector pairs in each bin. The color of each bar provides the standard deviation of detector pair angles within each bin. The bin containing $(170^\circ, 180^\circ]$, for example, is darkest because all pairs within that bin are at exactly 180° , producing the lowest standard deviation of 0° .

selected to minimize misclassification of photons as neutrons in the measurement, which mostly occurs below this threshold. An upper voltage limit reduced the experimental sensitivity to neutrons with energy depositions above 8.1 MeV. This work focuses on events where both detected neutrons have energies in the range 1 MeV to 4 MeV due to reduced statistics at higher energies.

2.2. Simulation Techniques

The experimental setup was simulated using MCNPX-PoliMi, which models the laboratory geometry and performs the particle transport. The system was modeled in great detail, including the Chi-Nu structure, concrete floor, and fission chamber. Waveform processing and particle-type classification is assumed to be perfect in the simulation so that all events are identified as the correct particle type. A light output threshold of 100 keVee was used to match that of the experimental data.

In order to study different fission models, CGMF, FREYA, and the built-in PoliMi source IPOL(1)=1, referred to as POLIMI, were used in MCNPX-PoliMi. The similarities and differences between FREYA and CGMF are discussed in a recent article [17], as well as some information about POLIMI. These models produced list-mode data including initial energy, initial direction, and particle type for each particle generated in an individual fission event, which was passed to MCNPX-PoliMi for

transport. Following transport, MCNPX-PoliMi produced a file with event-by-event information on interactions in detector cells. Detector response was calculated with MPPost post-processing software [16], which handles the nonlinear light output of organic scintillators.

POLIMI and FREYA simulated 10^9 fission events, while 1.92×10^8 CGMF events were employed, resampled with new, randomly sampled, fission fragment directions from a subset of 1.92×10^6 events. Table 1 shows these values and the number of detected bicorrelation events in all four datasets.

Table 1: Experimentally detected and generated fission events resulting in the given total and per fission bicorrelation counts.

	number fissions	bicorrelation counts	bicorrelation counts per fission
Experiment	1.42×10^9	$(3.941 \pm 0.002) \times 10^6$	$(2.771 \pm 0.002) \times 10^{-3}$
CGMF	1.92×10^8	$(0.737 \pm 0.085) \times 10^6$	$(1.786 \pm 0.004) \times 10^{-3}$
FREYA	1.00×10^9	$(2.978 \pm 0.002) \times 10^6$	$(2.978 \pm 0.002) \times 10^{-3}$
POLIMI	1.00×10^9	$(3.409 \pm 0.002) \times 10^6$	$(3.409 \pm 0.002) \times 10^{-3}$

2.3. Identifying Bicorrelation Events

This paper studies the relationship between pairs of detected neutrons that are emitted from the same fission event, as illustrated in Fig. 3. The interaction times of two neutrons, t_1 and t_2 , were each correlated with the corresponding fission chamber trigger time, t_0 , in the measured data. The time of flight of each neutron was calculated as $\Delta t_i = t_i - t_0$. In the MCNPX-PoliMi simulations, the times of flight were provided directly on an event-by-event basis in the output file. These double neutron events are referred to as “bicorrelation” events, a term first applied to coincident radiation counting by Mattingly [27] because both detected neutrons are correlated with the fission chamber trigger. Bicorrelation events were selected as any double neutron interaction within 200 ns of the fission time. If $n > 2$ prompt neutrons were detected, $\binom{n}{2}$ separate bicorrelation events were recorded: one from each pair of detectors. For example, if three neutrons were detected from the same fission event, then three pairs of neutrons were analyzed.

Bicorrelation events include interactions of prompt fission neutrons that travel straight to the detector, which are the *true* bicorrelation events, and events in which one or both of the neutrons comes from an accidental interaction such as room return, cross talk, and, in the case of experimental data, natural background. In our experiment, triggering in coincidence with the

143 fission chamber offers significant background suppression compared to other measurements that
 144 do not use a fission chamber signal. Background in bicorrelation events in this measurement was
 145 estimated to be less than 2.5% of the overall signal and had a negligible effect on the final results.
 146 We did not remove it in the analysis.

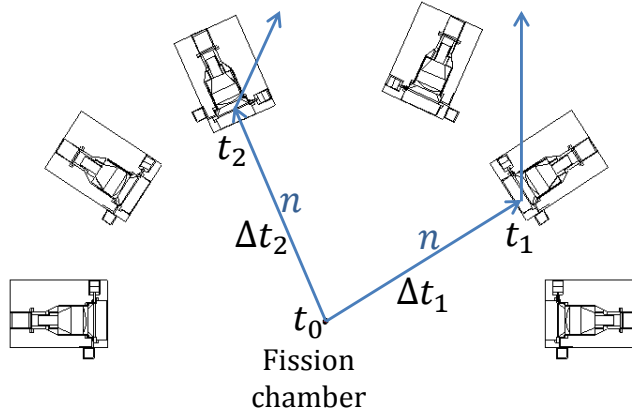


Figure 3: (Color online) Schematic of a true bicorrelation event in which two prompt fission neutrons are detected in coincidence with their originating fission. The schematic used is a two-dimensional view through an arc of the detector array in the MCNPX-PoliMi model.

147 This work will study the characteristics of bicorrelation events with respect to the angle between
 148 the neutrons; this will be referred to as the bicorrelation angle and is approximated as the angle
 149 between the centers of each detector with respect to the fission chamber.

150 2.4. The Bicorrelation Distribution

151 This analysis will make use of the bicorrelation distribution: a two-dimensional distribution
 152 of time of flight or energy for bicorrelation neutron events. The energies are calculated from the
 153 times of flight with the assumption that the neutron traveled directly from the fission chamber
 154 to the detector. Slight differences in the distances from the fission chamber to each detector
 155 are incorporated. Figure 4 shows the bicorrelation distributions for the experiment and POLIMI
 156 simulations. These distributions show the number of counts at each $(\Delta t_1, \Delta t_2)$ or (E_1, E_2) pixel,
 157 normalized by the number of detector pairs, the number of fission events, and the pixel size.

158 There are many interesting features in these distributions, a few of which are described here.
 159 The first observation is the primary feature produced by true prompt fission neutron bicorrelation
 160 events. In the time-of-flight distributions, this feature appears as a bright yellow spot within the

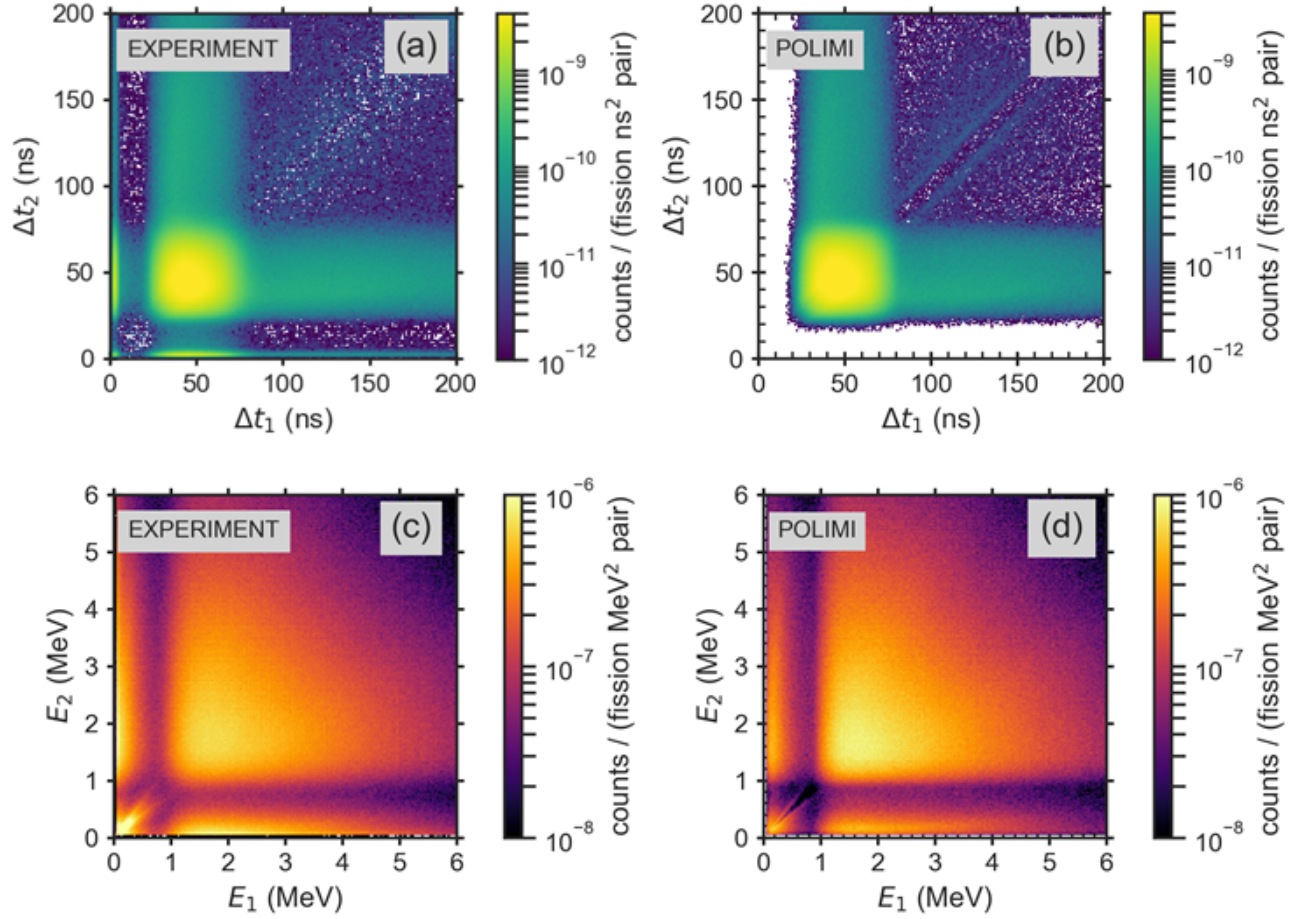


Figure 4: (Color online) Bicorrelation time-of-flight distribution for (a) experimental data and (b) POLIMI simulations, and bicorrelation energy distribution for (c) experimental data and (d) POLIMI simulations.

approximate time window $25 < \Delta t_i < 75$ ns. In the energy distributions, this feature appears as a bright distribution extending to larger neutron energies from approximately $E_i = 1$ MeV for each neutron, corresponding to the peak of the prompt fission neutron spectrum.

A second feature that can be observed in the bicorrelation distributions is the presence of accidental events, such as room return. In the time-of-flight distributions, these events appear at times beyond the true bicorrelation region, and dominate at $\Delta t_i > 75$ ns, where double-accidental events exist. Events in which a single accidental neutron is detected in coincidence with a true prompt fission neutron produce the wide bands emanating from the true bicorrelation region toward higher Δt_i . When converted to neutron energy, these long time-of-flight events are mapped to very low energies and appear on the bicorrelation energy distribution as the bright

171 yellow regions along the axes and as a bright spot at the origin.

172 A third feature visible in the experiment time-of-flight distributions is PSD misclassification,
173 which appears as the narrow bands along the x - and y -axes and as a localized spot at the origin.
174 In this case, one or both of the particles is a gamma ray with a very small Δt_i that has been
175 misclassified as a neutron. While this feature in the time-of-flight distribution is very similar to
176 the accidental event features in the energy distribution, they are, in fact, different. This feature
177 due to misclassification does not appear in the POLIMI distribution, as all simulations assume
178 perfect PSD and thus do not include misclassified events.

179 A final feature that is barely visible in these time-of-flight distributions is cross talk. This
180 effect is explored in more detail in the next section.

181 2.5. Cross Talk

182 Cross talk occurs when the same neutron interacts in multiple detectors and produces a false
183 bicornelation event. Cross talk is prevalent in detector pairs with small angular separation. Because
184 full simulations were performed for all fission event generators, cross-talk events are present in all
185 simulations and in the experimental data. Although it is possible to remove cross talk on an
186 average basis, as performed in Ref. [28], there is no way to remove cross talk on an event-by-event
187 basis in experimental data. Therefore, cross-talk events and their effects on the bicornelation
188 analysis are present and will be discussed throughout this work.

189 Cross-talk events can be visually identified on small-angle bicornelation distributions, as shown
190 in Fig. 5 for a POLIMI simulation of detector pairs at 15° and 45° . Cross-talk events appear
191 as two diagonal bands in the bicornelation time-of-flight and energy distributions. The line of
192 cross talk can be defined as $\Delta t_2 = \Delta t_1 + \Delta t_{1 \rightarrow 2}$ when the neutron interacts first in detector 1,
193 and $\Delta t_{1 \rightarrow 2}$ is the time-of-flight between detectors. Likewise, $\Delta t_1 = \Delta t_2 + \Delta t_{2 \rightarrow 1}$ describes the
194 line of cross-talk events in which the neutron interacted first in detector 2. Then $\Delta t_{1 \rightarrow 2}$ will
195 follow a distribution according to the energies of neutrons traveling from detector 1 to detector
196 2 and the distance between them. Thus, the $(\Delta t_2, \Delta t_1)$ distribution will be diagonal lines with
197 widths determined by the $\Delta t_{1 \rightarrow 2}$ distribution and offset from the identify line $\Delta t_2 = \Delta t_1$ by the
198 magnitude of $\Delta t_{1 \rightarrow 2}$. As the angle and distance between detectors increases, $\Delta t_{1 \rightarrow 2}$ increases and

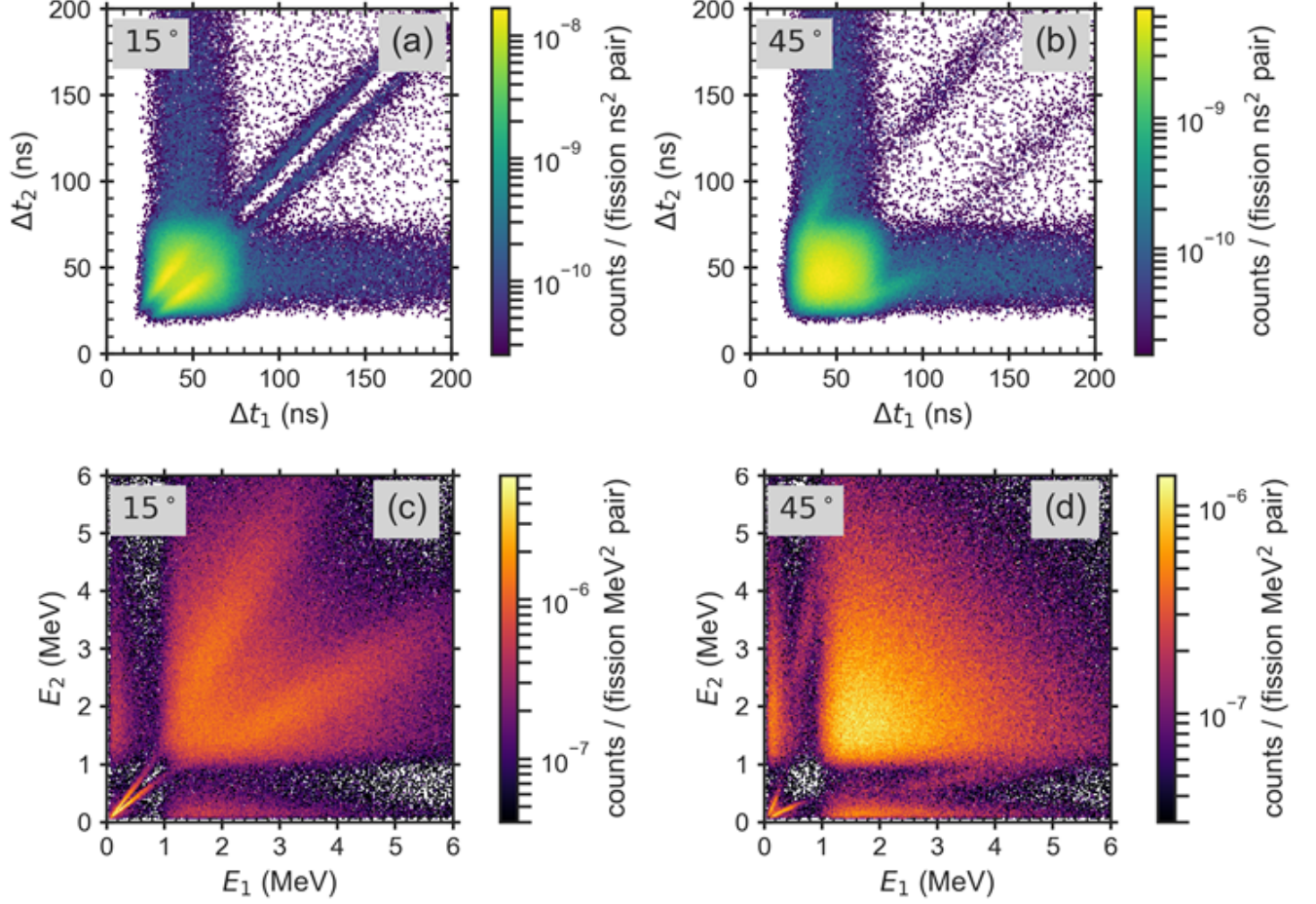


Figure 5: (Color online) Bicornelation (a,b) time-of-flight and (c,d) energy distributions from POLIMI simulation showing cross-talk effects, displayed for detector pairs at (a,c) 15° and (b,d) 45° . The diagonal bands in each distribution include cross-talk events, which move farther from the identity line ($\Delta t_1 = \Delta t_2$ and $E_1 = E_2$) and decrease in magnitude as the angle between detectors increases.

the cross-talk bands decrease in magnitude and departs farther from the identity line $\Delta t_2 = \Delta t_1$. The cross-talk features at long times (> 75 ns) and low energies (< 1 MeV) are largely due to accidental cross-talk events from room return or background.

Cross-talk effects are prominent at 15° and visible in some distributions up to 75° . Regions that may be affected by cross talk are displayed with gray background in the analysis plots in the next section.

3. Analysis and Results

3.1. Anisotropy in Neutron Emission Rate

Neutron emission from ^{252}Cf spontaneous fission is assumed to occur after the fission fragments are in motion and traveling in opposite directions [29], assuming all neutrons are emitted from fully-accelerated fragments. Scission neutrons, emitted isotropically in the ^{252}Cf rest frame and estimated to be 0 – 20% of prompt neutron emission [12, 31, 32], are not included in the models or simulations discussed here.

In our simulations, we assume that neutron emission is isotropic in the rest frame of each fission fragment but anisotropic in the laboratory frame of motion. Thus, the direction of neutron emission follows that of the fission fragment that emitted it so that neutrons emitted in the direction of the fission fragment will receive an energy boost. The anisotropy can be characterized by calculating the count rate of bicorrelation events in detector pairs as a function of bicorrelation angle. The relative bicorrelation count rate, W_{ij} , for each pair of detectors i and j , is defined as [20]

$$W_{ij} = \frac{D_{ij}}{S_i S_j} \quad (1)$$

where D_{ij} is the doubles count rate, and S_i and S_j are the corresponding singles count rates. Each of these rates are determined from the number of counts in the energy range 1 MeV to 4 MeV. This conservative energy range was selected to minimize threshold effects at low energies and gamma-ray misclassification at higher energies while maximizing statistics. This analysis corrects for slight variations in efficiency between detectors.

An average W was calculated for detector pairs in each 10° bin, $\overline{W}(\theta)$. Figure 6(a) shows $\overline{W}(\theta)$ for all four data sets, normalized by the integral over the distribution. The angle is plotted at the midpoint of the bins. For example, the data points at 15° include all pairs in the range $(10^\circ, 20^\circ]$. The error in $\overline{W}(\theta)$ was calculated as the standard deviation of W_{ij} values in that angular range, and is influenced by the variation in W and the angular distribution in detector pair angles in that range. The error bar on the data point at 25° , for instance, is larger than most others, because the detector pairs in that bin are more evenly distributed across the represented angle range, as

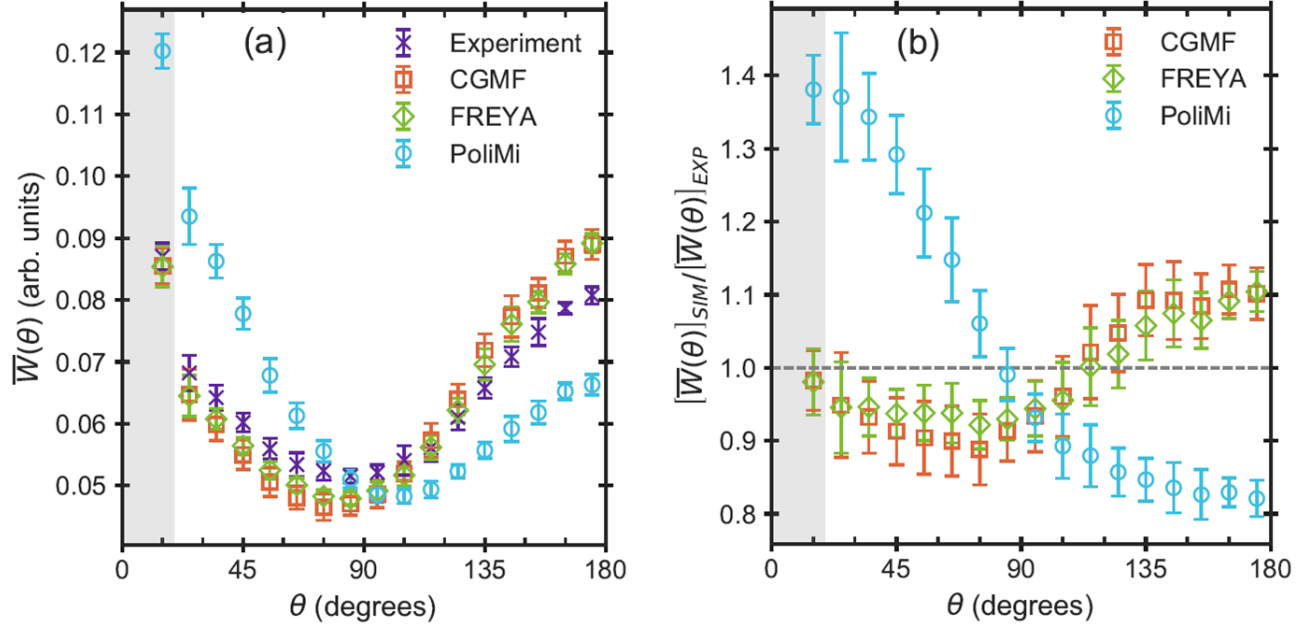


Figure 6: (Color online) (a) Relative bicorrelation count rate $\overline{W}(\theta)$ for events from 1 MeV to 4 MeV, normalized by integral. (b) Ratio between relative bicorrelation rate for each simulation to that from experiment. The gray region from 0° to 20° serves as a reminder that cross talk is significant over this range.

illustrated by the standard deviation in Fig. 2 and the slope of $\overline{W}(\theta)$ is high in that region. This error is larger than the propagated statistical error and attempts to incorporate systematic errors.

All four datasets in Fig. 6(a) produce smoothly-varying distributions with a local maximum at 15° where cross talk is prevalent, a minimum near 90° , and a local maximum at 175° . The minimum angle varies from 75° for CGMF to 85° for FREYA and the experiment to 105° in POLIMI. The experimental result and the POLIMI simulation agree within uncertainties with previous work with lower angular resolution [4]. The largest magnitude of change between $\overline{W}(175^\circ)$ and $\overline{W}(85^\circ)$ is found with CGMF, while the smallest magnitude of change is seen in POLIMI.

The most striking difference is that the POLIMI result is tilted to the left, while the CGMF, FREYA, and experimental results are tilted to the right. The tilt of the angular correlation is strongly tied to the sharing of excitation energy between fission fragments. The complete event models CGMF and FREYA handle this sharing by giving some additional energy to the light fragment. In FREYA, this is done with the x parameter, defined as the advantage in excitation energy given to the light fragment [12], where x is an adjustable input parameter expected to be larger than 1. The best fit value of x for FREYA with ^{252}Cf (sf) was found to be 1.27 [33].

246 In **CGMF**, the energy sharing is done in a similar way except that the x parameter is not a single
 247 value but is based on the ratio of neutron multiplicities of the light and heavy fragment pairs as
 248 a function of fragment mass, $R_T(A)$, to match the $\nu(A)$ data. When a single value of R_T is used,
 249 the resulting $\nu(A)$ is similar to that of **FREYA** with $x = 1.27$ [34].

250 A larger value of x makes the distribution tilt toward 0° as the light fragment receives more
 251 energy and emits more neutrons, increasing the zero degree correlation. A value of x near 1
 252 makes the distribution tilt more strongly toward 180° as the energy is split more evenly between
 253 fragments. The **POLIMI** result corresponds to $x \sim 2$, giving the light fragment twice as much
 254 energy as the heavy fragment which is not physically realistic. This discrepancy is a side effect
 255 of how **POLIMI** samples each quantity independently and does not capture effects related to the
 256 de-excitation process.

257 Figure 6(b) shows $\overline{W}(\theta)$ from each simulation divided by that for experiment. This ratio shows
 258 that, compared to the measured results, **POLIMI** overpredicts $\overline{W}(\theta)$ by up to 90% at low angles and
 259 underpredicts at high angles, while **CGMF** and **FREYA** underpredict at low angles and overpredict at
 260 high angles by a much smaller amount, about 10% in each case. This discrepancy may indicate
 261 that **CGMF** and **FREYA** predict too many two-neutron events in which one neutron comes from one
 262 fragment and the other neutron from the complementary fragment, as opposed to both neutrons
 263 coming from the same fragment.

264 This variation can be explored further by capturing the magnitude of the anisotropy as a
 265 one-dimensional parameter A_{sym}

$$A_{\text{sym}} = \frac{W(180)}{W(90)} \approx \frac{\overline{W}(175^\circ)}{\overline{W}(85^\circ)}. \quad (2)$$

266 Due to the 10° wide discretization of angles, the data are compared at 175° and 85° , which include
 267 pairs at $(170^\circ, 180^\circ]$ and $(80^\circ, 90^\circ]$, respectively.

268 The anisotropy in neutron energy can be observed by varying the neutron energy threshold, as
 269 shown in Fig. 7. The magnitude of the anisotropy increases as the energy threshold is increased
 270 and lower energy neutrons are omitted from the analysis. This increase occurs because neutrons
 271 detected at angles near 180° are likely emitted from different fission fragments in their direction

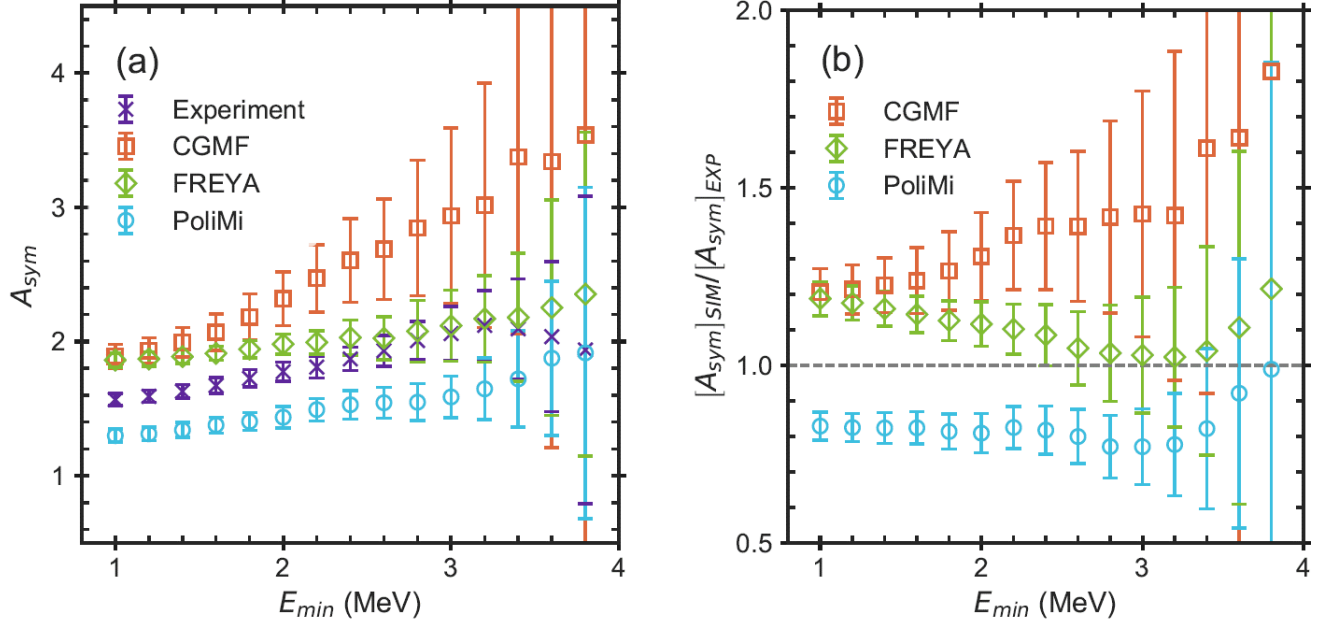


Figure 7: (Color online) (a) Magnitude of the neutron emission anisotropy, A_{sym} , as a function of E_{min} and (b) ratio between simulated results and measured data. The magnitude of anisotropy increases as the neutron population is limited to higher energies. The error bars increase with E_{min} as fewer events are included in the analysis, worsening statistics.

of travel and therefore receive a boost in energy due to the direction of motion. This boost also occurs for neutron pairs emitted at 0° , however, the Chi-Nu array cannot identify events at 0° where two neutrons interact in the same detector. Neutrons detected at angles near 90° did not receive this boost and therefore are emitted with lower energies. Thus, as the energy threshold is increased, events at angles near 90° are more likely to be removed from the population than events at 180° , thereby increasing A_{sym} .

Figure 7(a) shows that CGMF consistently produces the highest values of A_{sym} while POLIMI consistently produces the lowest. Note also that the uncertainties grow as E_{min} increases because there are fewer events in the population, limiting statistics. Figure 7(b) shows the ratio of each of the simulations to the experimental data. This ratio is roughly independent of E_{min} at ~ 0.8 for POLIMI, while CGMF and FREYA vary slightly as E_{min} increases. The FREYA ratio starts at ~ 1.2 and drops toward to 1 as E_{min} increases, while the CGMF ratio starts at 1.2 and grows larger with increasing E_{min} .

3.2. Neutron Energy Characteristics

As stated in Sec. 3.1, the energies of prompt fission neutrons vary with their direction of emission relative to the direction of fission fragment motion. In detected bicorrelation events, this boost increases the average detected energies of pairs near 180°, which are likely to be emitted from opposite fragments in the fragment direction of motion. One can observe this effect by calculating the average neutron energy for neutrons in the 1 to 4 MeV range detected in bicorrelation events, defined as

$$\overline{E}_n = (\overline{E_1} + \overline{E_2})/2. \quad (3)$$

and shown as a function of bicorrelation angle in Fig. 8(a). As stated in Sec. 3.1, this energy range is chosen to remove events at low energies that may have threshold effects and events at high energies that are gamma rays misclassified as neutrons. This average energy calculation does not provide a measurement of the average energy of the entire neutron population, but rather that in the 1 to 4 MeV range as a benchmark for comparison. This distribution shows that, in all cases, the average neutron energy reaches a minimum near 90° and increases steadily until it reaches a local maximum at 180°. Note that \overline{E}_n is higher than expected at 15° due to cross-talk effects; the gray band for angles less than 20° is a reminder of this.

Although the shapes are approximately the same in all cases for angles less than 90°, the behavior varies greatly above 90°. First, the minimum \overline{E}_n for **CGMF** occurs at 85° while for all other results it is at 95°. Second, **CGMF** has the steepest increase in \overline{E}_n at angles up to 180°. Third, the experimental results are in excellent agreement with **FREYA** at angles below 125°, but the value of \overline{E}_n for **FREYA** levels out at higher angles while the \overline{E}_n of the data continues to rise.

Figure 8(b) shows the ratio between each simulation and experiment, demonstrating that the agreement among all results is very good, as all simulations are within 3% of the experimental data. **POLIMI** produces consistently lower energies than experiment while **CGMF** produces lower energies below 135° and higher energies above 135°. **FREYA** agrees with experiment below 125°, but it produces lower average energies above this angle.

While Fig. 8 provides a measurement of the energy distribution across the entire neutron

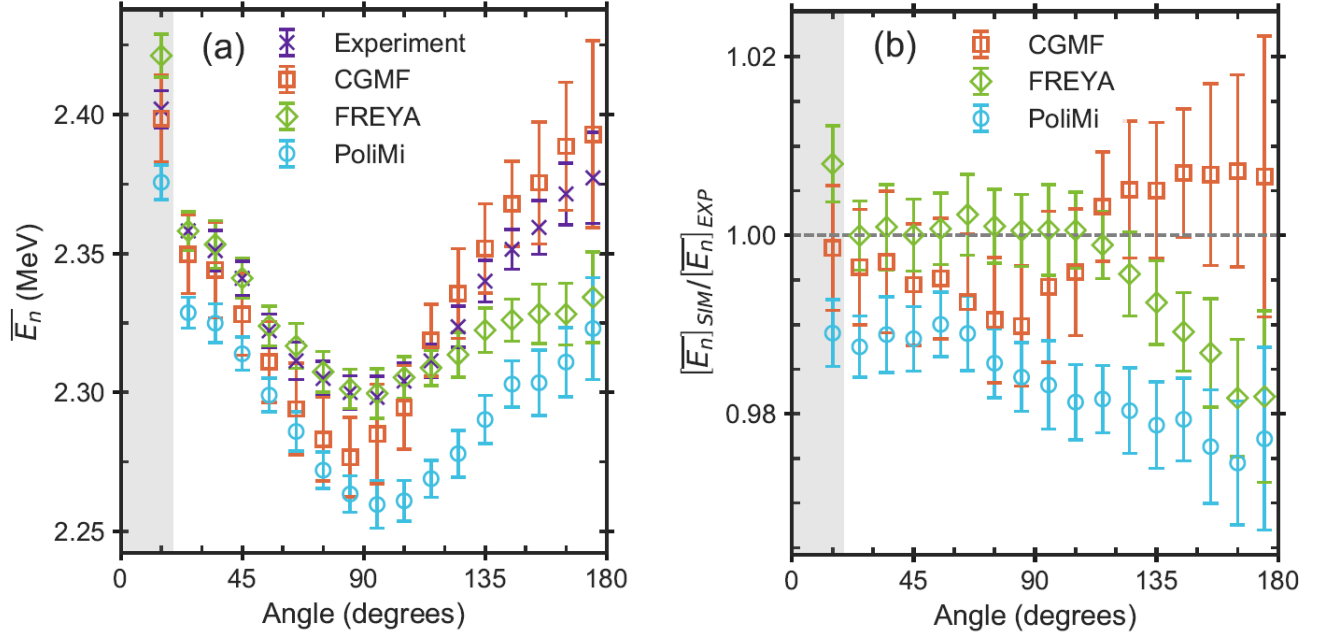


Figure 8: (Color online) (a) Average neutron energy as a function of bicornelation angle across a range of 1 MeV to 4 MeV. (b) Ratio between average simulated energy and average measured energy, demonstrating agreement within 3% across all data. The gray region from 0° to 20° serves as a reminder that cross talk is significant over this range.

population, it does not demonstrate whether the energy of one neutron depends on the energy of its bicornelation partner. To determine this dependence, for fixed E_i of 2 MeV and 3 MeV, the average energy \bar{E}_j of the partner neutron is shown as a function of θ in Fig. 9.

The distributions shown in Fig. 9 share the same features as in Fig. 8(a), although the behavior of data at angles less than 30° varies due to the effect of cross talk on E_i . In fact, no significant angular dependence was observed in the shape of \bar{E}_n or \bar{E}_j at any E_i .

Some differences were seen, however, in the values of \bar{E}_j as E_i is varied. The dependence of \bar{E}_j on E_i can be enhanced by studying \bar{E}_j as a function of E_i at a fixed bicornelation angle, as shown in Fig. 10. Figure 10 (a)-(c) shows $\bar{E}_j(E_i)$ at bicornelation angles 85°, 135°, and 175°. While it is not immediately clear to the naked eye whether a dependence of \bar{E}_j on E_i exists, one can perform a least-squares linear regression on the data and determine whether there is a statistically significant nonzero slope, m , as shown in Fig. 10(d). Angles below 85° are omitted, because cross talk was shown to be significant enough to contaminate the calculation of the slope at lower angles.

The error bars in Figs. 8, 9, and 10 vary firstly with sample size and are smaller in angle bins

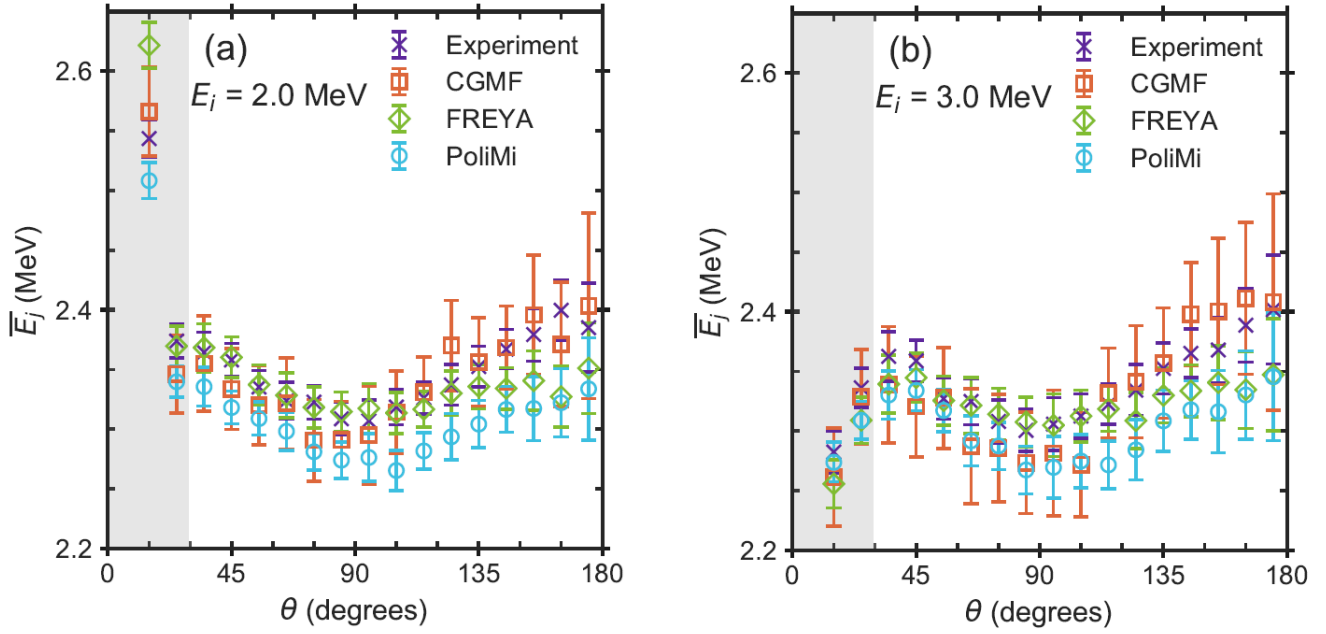


Figure 9: (Color online) Average energy of neutrons across a range of 1 MeV to 4 MeV detected in coincidence with a (a) 2 MeV and (b) 3 MeV neutron.

with more detector pairs. Error bars are largest in the two highest angle bins, which have the lowest number of detector pairs, as shown in Fig. 2.

There are several interesting aspects of this distribution. First and foremost, all four results have slopes within 2σ of $m = 0.0$ across all angles. Thus, there is no statistically significant slope in any of the datasets. However, trends do exist in the data which will be discussed here and will be the subject of future work in order to reduce uncertainties and determine whether the trends are significant.

All results, data and simulations, show a negative slope near 90° . Above 140° , the slope of the data, as well as that of the CGMF and POLIMI simulations, becomes positive, crossing zero near 135° . Since events with bicorrelation angle near 90° are likely emitted from the same fragment, the negative slope at angles near 90° could indicate that neutrons emitted from the same fission fragment compete with one another for energy. Events with neutrons emitted near 180° are likely to come from different fission fragments, indicating that there may be some positive correlation in neutron energies emitted from different fission fragments. Note that, the FREYA simulation results in negative slope across all angles, indicating that correlated neutrons produced by FREYA may

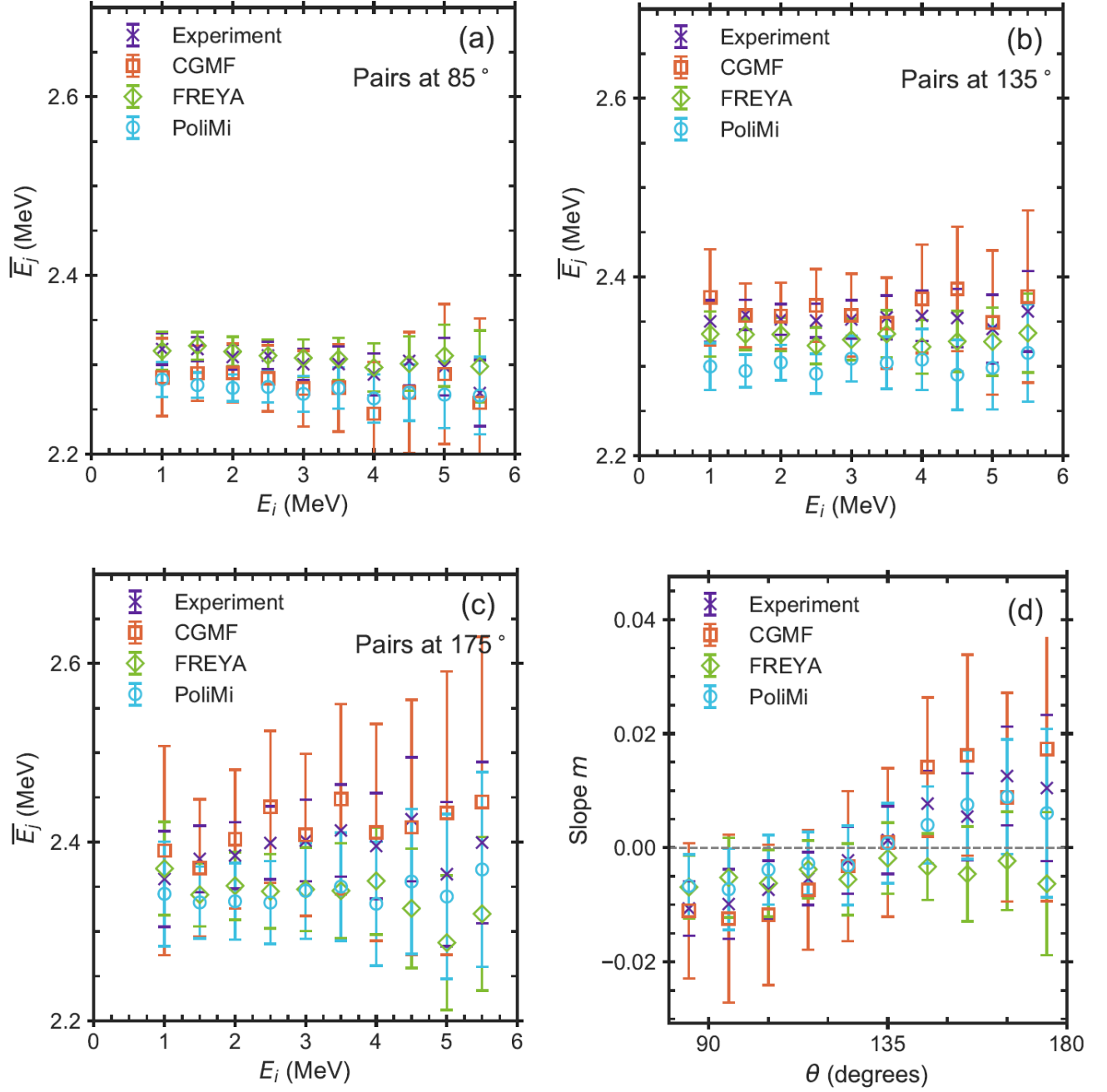


Figure 10: (Color online) Average correlated neutron energy \overline{E}_j for fixed energy E_i for detector pairs at (a) 85°, (b) 135°, and (c) 175°, and (d) slope of least-squares fit to $\overline{E}_j(E_i)$ at angles 85° and higher.

340 compete with one another for energy regardless of whether or not they were produced by the same
 341 fission fragment.

342 4. Conclusion

343 This work investigated correlations in angle and energy between prompt neutrons emitted in
344 the same ^{252}Cf spontaneous fission event, including measuring the energy dependence between
345 correlated neutrons for the first time. Experiments were performed using 42 components of the
346 Chi-Nu detector array in a hemispherical configuration surrounding a fission chamber. The de-
347 tector array was simulated in MCNPX-PoliMi with three different fission models: MCNPX-POLIMI
348 IPOL(1)=1, CGMF, and FREYA.

349 Characteristics of the correlated neutrons were studied with respect to the angle between the
350 two neutrons. The large number of detectors produced a broad distribution of bicorrelation angles
351 collected into 10° bins. The 1 m flight path allowed for experimental timing resolution as low as
352 1 ns, allowing excellent energy resolution to be attained for neutron energies between 1 MeV and
353 4 MeV from the time-of-flight calculations.

354 The simulations showed good agreement with experiment for all measured quantities, while
355 revealing interesting differences between fission event generators. The neutron emission anisotropy
356 generated by CGMF and FREYA agreed within 10% of experiment, while underpredicting the anisotropy
357 at small angles and overpredicting it at high angles. On the other hand, POLIMI showed poor agree-
358 ment, differing up to 40% from experiment at low angles. All simulated average neutron energies
359 fell within 3% of the experimental data. FREYA produced the best agreement with experiment:
360 the average neutron energies agreed with the data to 0.5% for angles below 135° .

361 The average neutron energy was found to be negatively correlated with the energy of its
362 correlated partner for pairs at 85° , indicating that neutrons may compete for emission energy
363 at low angles, where neutrons are likely to be emitted from the same fission fragment. This
364 correlation was found to be positive for pairs at 175° , where neutrons are likely to be emitted from
365 different fission fragments. However, this result is inconclusive because the uncertainties in the
366 measurements result in calculated slopes within 2σ of 0. Further experiments should be performed
367 to study this effect in greater detail.

368 These conclusions lead to further questions that could be pursued by more sophisticated ex-
369 periments. The ability to distinguish events with neutrons from the same fission fragment would

determine whether there is a competition for energy within the energy spectrum of the fragment, such as a reduction in the average emission energy for each subsequent neutron emission. Tracking the fission fragments would allow this analysis to be repeated with respect to the fission fragment motion. Additionally, that would also enable experimental measurement of differences due to energy sharing between fragments of $\nu(A)$, $\epsilon(A)$ (where ϵ is the average neutron kinetic energy), $\nu(\text{TKE})$, and neutron-light fragment correlations, specifically for a given A_L . A comparison of these results are shown from FREYA and CGMF in Ref. [17]. Extracting information about the neutrons at the time of their emission from the fragments, as opposed to relying on the information gleaned from the neutrons arriving at the detectors, which may have undergone some rescattering, would enable more direct comparison to the complete fission event models. Finally, repeating this measurement with ^{240}Pu (sf), with an average neutron multiplicity closer to 2 (~ 2.15) than ^{252}Cf (sf) ($\bar{\nu} \sim 3.76$), would reduce the number of fission events with multiple neutron pairs in the same event. Thus, in this case, detected bicorrelation events are more likely to come from events where exactly two neutrons are emitted: either one from each fragment or two from the same fragment.

Acknowledgments

This work was performed under the auspices of the U.S. Department of Energy by Los Alamos National Security, LLC, under Contract No. DE-AC52-06NA25396, by Lawrence Livermore National Security, LLC under Contract No. DE-AC52-07NA27344, by Lawrence Berkeley National Laboratory under Contract DE-AC02-05CH11231, by the Consortium for Verification Technology under Contract No. DE-NA0002534, by the Office of Nuclear Physics in the Office of Science under Contract No. DE-AC02-05CH11231, and by the University of Michigan.

- [1] J. S. Fraser, The angular distribution of prompt neutrons emitted in fission, Physical Review 88 (3) (1952) 536–541. [doi:10.1103/PhysRev.88.536](https://doi.org/10.1103/PhysRev.88.536).
- [2] K. Skarsvag, Time distribution of gamma-rays from spontaneous fission of Cf-252, Nuclear Physics A 153 (1970) 82–96. [doi:10.1016/0375-9474\(70\)90757-8](https://doi.org/10.1016/0375-9474(70)90757-8).
- [3] H. R. Bowman, S. G. Thompson, J. C. D. Milton, W. J. Swiatecki, Velocity and angular

distributions of prompt neutrons from spontaneous fission of Cf252, Physical Review 126 (6) (1962) 2120–2136. [doi:10.1103/PhysRev.126.2120](https://doi.org/10.1103/PhysRev.126.2120).

[4] S. Pozzi, B. Wieger, A. Enqvist, S. Clarke, M. Flaska, M. Marcath, E. Larsen, R. Haight, E. Padovani, Correlated Neutron Emissions from 252Cf, Nuclear Science and Engineering 178 (2) (2014) 250–260. [doi:10.13182/NSE13-96](https://doi.org/10.13182/NSE13-96).

[5] S. Pozzi, S. Clarke, W. Walsh, E. Miller, J. Dolan, M. Flaska, B. Wieger, A. Enqvist, E. Padovani, J. Mattingly, D. Chichester, P. Peerani, MCNPX-PoliMi for nuclear non-proliferation applications, Nuclear Instruments and Methods in Physics Research Section A: Accelerators, Spectrometers, Detectors and Associated Equipment 694 (2012) 119–125. [doi:10.1016/J.NIMA.2012.07.040](https://doi.org/10.1016/J.NIMA.2012.07.040).

[6] P. Talou, T. Kawano, I. Stetcu, Prompt Fission Neutrons and Gamma Rays in a Monte Carlo Hauser-Feshbach Formalism, Physics Procedia 47 (2013) 39–46. [doi:10.1016/J.PHPR0.2013.06.007](https://doi.org/10.1016/J.PHPR0.2013.06.007).

[7] P. Talou, I. Stetcu, T. Kawano, Modeling the Emission of Prompt Fission γ Rays for Fundamental Physics and Applications, Physics Procedia 59 (2014) 83–88. [doi:10.1016/J.PHPR0.2014.10.013](https://doi.org/10.1016/J.PHPR0.2014.10.013).

[8] P. Talou, T. Kawano, I. Stetcu, J. P. Lestone, E. McKigney, M. B. Chadwick, Late-time emission of prompt fission γ rays, Physical Review C 94 (6) (2016) 064613. [doi:10.1103/PhysRevC.94.064613](https://doi.org/10.1103/PhysRevC.94.064613).

[9] J. Randrup, R. Vogt, Calculation of fission observables through event-by-event simulation, Physical Review C 80 (2) (2009) 024601. [doi:10.1103/PhysRevC.80.024601](https://doi.org/10.1103/PhysRevC.80.024601).

[10] R. Vogt, J. Randrup, Event-by-event study of neutron observables in spontaneous and thermal fission, Physical Review C 84 (4) (2011) 044621. [doi:10.1103/PhysRevC.84.044621](https://doi.org/10.1103/PhysRevC.84.044621).

[11] R. Vogt, J. Randrup, Event-by-event study of photon observables in spontaneous and thermal fission, Physical Review C 87 (4) (2013) 044602. [doi:10.1103/PhysRevC.87.044602](https://doi.org/10.1103/PhysRevC.87.044602).

- [12] R. Vogt, J. Randrup, Neutron angular correlations in spontaneous and neutron-induced fission, *Physical Review C* 90 (6) (2014) 064623. [doi:10.1103/PhysRevC.90.064623](https://doi.org/10.1103/PhysRevC.90.064623).
- [13] J. Randrup, R. Vogt, Refined treatment of angular momentum in the event-by-event fission model *freya*, *Physical Review C* 89 (4) (2014) 044601. [doi:10.1103/PhysRevC.89.044601](https://doi.org/10.1103/PhysRevC.89.044601).
- [14] R. Vogt, J. Randrup, Improved modeling of photon observables with the event-by-event fission model *freya*, *Physical Review C* 96 (6) (2017) 064620. [doi:10.1103/PhysRevC.96.064620](https://doi.org/10.1103/PhysRevC.96.064620).
- [15] J. Verbeke, J. Randrup, R. Vogt, Fission Reaction Event Yield Algorithm FREYA 2.0.2, *Computer Physics Communications* 222 (2018) 263–266. [doi:10.1016/J.CPC.2017.09.006](https://doi.org/10.1016/J.CPC.2017.09.006).
- [16] E. C. Miller, S. D. Clarke, M. Flaska, S. A. Pozzi, E. Padovani, *Journal of nuclear materials management.*, Vol. 40, Institute of Nuclear Materials Management, 2012.
- [17] P. Talou, *et al.*. Correlated Prompt Fission Data in Transport Simulations, *Eur. Phys. J. A* 54 (2018) No. 1, 9. [doi:10.1140/epja/i2018-12455-0](https://doi.org/10.1140/epja/i2018-12455-0).
- [18] K. Frame, W. Clay, T. Elmont, E.-I. Esch, P. Karpus, D. MacArthur, E. McKigney, P. Santi, M. Smith, J. Thron, R. Williams, Development of a liquid scintillator neutron multiplicity counter (LSMC), *Nuclear Instruments and Methods in Physics Research Section A: Accelerators, Spectrometers, Detectors and Associated Equipment* 579 (1) (2007) 192–195. [doi:10.1016/j.nima.2007.04.038](https://doi.org/10.1016/j.nima.2007.04.038).
- [19] A. Di Fulvio, T. Shin, T. Jordan, C. Sosa, M. Ruch, S. Clarke, D. Chichester, S. Pozzi, Passive assay of plutonium metal plates using a fast-neutron multiplicity counter, *Nuclear Instruments and Methods in Physics Research Section A: Accelerators, Spectrometers, Detectors and Associated Equipment* 855 (2017) 92–101. [doi:10.1016/j.nima.2017.02.082](https://doi.org/10.1016/j.nima.2017.02.082).
- [20] J. M. Mueller, J. Mattingly, Using anisotropies in prompt fission neutron coincidences to assess the neutron multiplication of highly multiplying subcritical plutonium assemblies, *Nuclear Instruments and Methods in Physics Research, Section A: Accelerators, Spectrometers, Detectors and Associated Equipment* 825 (2016) 87–92. [doi:10.1016/j.nima.2016.04.027](https://doi.org/10.1016/j.nima.2016.04.027).

- [21] L. Holewa, W. Charlton, E. Miller, S. Pozzi, Using neutron angular anisotropy information to dynamically determine the ratio of the (α, n) rate to spontaneous fission rate for coincidence counting applications, Nuclear Instruments and Methods in Physics Research, Section A: Accelerators, Spectrometers, Detectors and Associated Equipment 701 (2013) 249–253. doi:10.1016/j.nima.2012.11.026.
- [22] B. Perdue, T. Taddeucci, R. Haight, T. Bredeweg, M. Devlin, N. Fotiades, M. Jandel, A. Laptev, H. Lee, R. Nelson, J. O'Donnell, J. Ullmann, S. Wender, C. Wu, E. Kwan, A. Chyzh, R. Henderson, J. Gostic, Development of an Array of Liquid Scintillators to Measure the Prompt Fission Neutron Spectrum at LANSCE, Nuclear Data Sheets 119 (2014) 371–372. doi:10.1016/j.nds.2014.08.102.
- [23] M. J. Marcath, (2018). Measured and Simulated Prompt Fission Neutron and Photon Correlations. University of Michigan. Retrieved from <https://deepblue.lib.umich.edu/handle/2027.42/147560>
- [24] J. M. Verbeke, L. F. Nakae, R. Vogt, Neutron-neutron angular correlations in spontaneous fission of Cf252 and Pu240, Physical Review C 97 (4) (2018) 044601. doi:10.1103/PhysRevC.97.044601.
- [25] M. J. Marcath, R. C. Haight, R. Vogt, M. Devlin, P. Talou, I. Stetcu, J. Randrup, P. F. Schuster, S. D. Clarke, S. A. Pozzi, Measured and simulated 252Cf(sf) prompt neutron-photon competition, Physical Review C 97 (4) (2018) 1–15. doi:10.1103/PhysRevC.97.044622.
- [26] J. Polack, M. Flaska, A. Enqvist, C. Sosa, C. Lawrence, S. Pozzi, An algorithm for charge-integration, pulse-shape discrimination and estimation of neutron/photon misclassification in organic scintillators, Nuclear Instruments and Methods in Physics Research Section A: Accelerators, Spectrometers, Detectors and Associated Equipment 795 (2015) 253–267. doi:10.1016/j.nima.2015.05.048.
- [27] J. Mattingly, High Order Statistical Signatures from Source-Driven Measurements of Sub-critical Fissile Systems, Ph.D. thesis, The University of Tennessee, Knoxville (1998).

- [28] M. Marcath, T. Shin, S. Clarke, P. Peerani, S. Pozzi, Neutron angular distribution in plutonium-240 spontaneous fission, *Nuclear Instruments and Methods in Physics Research, Section A: Accelerators, Spectrometers, Detectors and Associated Equipment* 830 (2016) 163–169. [doi:10.1016/j.nima.2016.05.064](https://doi.org/10.1016/j.nima.2016.05.064).
- [29] A. Vorobyev, O. Shcherbakov, Y. Pleva, A. Gagarski, G. Val'ski, G. Petrov, V. Petrova, T. Zavarukhina, Measurements of angular and energy distributions of prompt neutrons from thermal neutron-induced fission, *Nuclear Instruments and Methods in Physics Research Section A: Accelerators, Spectrometers, Detectors and Associated Equipment* 598 (3) (2009) 795–801. [doi:10.1016/j.nima.2008.10.017](https://doi.org/10.1016/j.nima.2008.10.017).
- [30] R. B. Oberer, Maximum Alpha To Minimum Fission Pulse Amplitude for a Parallel-Plate and Hemispherical Cf-252 Ion-Chamber Instrumented Neutron Source, Oak Ridge National Laboratory Technical Report No. ORNL/TM-2000/290, 2000 (unpublished).
- [31] G. A. Petrov, H. Goutte, H. Faust, G. Fioni, D. Goutte, Current status of the search for scission neutrons in fission and estimation of their main characteristics, *AIP Conference Proceedings* 798 (2005) 205–212. [doi:10.1063/1.2137248](https://doi.org/10.1063/1.2137248).
- [32] A. Chietera, L. Stuttgé, F. Gönnerwein, Y. Kopatch, M. Mutterer, A. Gagarski, I. Guseva, E. Chernysheva, F. J. Hambsch, F. Hanappe, Z. Mezentseva, S. Telezhnikov, Angular correlations in the prompt neutron emission of spontaneous fission of ^{252}Cf , *The European Physical Journal A* 54 (6) (2018) 98. [doi:10.1140/epja/i2018-12529-y](https://doi.org/10.1140/epja/i2018-12529-y).
- [33] J. Van Dyke, L. Bernstein, R. Vogt, Parameter Optimization and Uncertainty Analysis of FREYA for Spontaneous Fission (2018) 1–13. [arXiv:1809.05587](https://arxiv.org/abs/1809.05587).
- [34] P. Talou, B. Becker, T. Kawano, M. B. Chadwick, Y. Danon, Advanced Monte Carlo modeling of prompt fission neutrons for thermal and fast neutron-induced fission reactions on ^{239}Pu , *Physical Review C* 83, 064612 (2011). [doi:10.1103/PhysRevC.83.064612](https://doi.org/10.1103/PhysRevC.83.064612)